

1978

Electron spin relaxation and tunnelling methyl groups

Peter A. Beckmann

Bryn Mawr College, pbeckman@brynmawr.edu

S. Clough

[Let us know how access to this document benefits you.](#)

Follow this and additional works at: https://repository.brynmawr.edu/physics_pubs



Part of the [Physics Commons](#)

Custom Citation

Beckmann, P. A. and S. Clough. 1978. "Electron spin relaxation and tunnelling methyl groups." *Journal of Physics C: Solid State Physics* 11.19: 4055-4067.

This paper is posted at Scholarship, Research, and Creative Work at Bryn Mawr College. https://repository.brynmawr.edu/physics_pubs/136

For more information, please contact repository@brynmawr.edu.

Electron spin relaxation and tunnelling methyl groups

Peter Beckmann† and Stan Clough

Department of Physics, University of Nottingham, Nottingham NG7 2RD, UK

Received 4 April 1978

Abstract. We have studied the energy transfer between free radicals and nearby tunnelling methyl groups near the resonant condition that the electron Larmor frequency and the methyl tunnelling frequency are equal. The measurements were made in a γ -irradiated single crystal of 4-methyl-2,6-ditertiarybutylphenol (MDBP) at 4.2 K and consisted of saturating the ESR signal and observing its return to equilibrium. This has been done at eleven ESR frequencies in the range $8.97 < \nu_s < 9.63$ GHz and for saturation times of 5, 50 and 200 s. We have developed a theoretical model for the non-exponential recovery which assumes that all the 4-methyl groups of the molecules surrounding a free radical have the same tunnelling rotation frequency ν_t and that the only coupling between the electrons and the methyl groups is the intermolecular dipole-dipole interaction. The agreement between theory and experiment is good where the resonance condition is satisfied but there is substantial disagreement where the resonance condition is not met. This suggests the need for more realistic models of the tunnelling frequency distribution and perhaps the need for additional electron-methyl-group interactions.

1. Introduction

Electron spin relaxation is a very sensitive technique for the investigation of molecular structure and dynamics in materials containing tunnelling methyl groups. We report here a detailed experimental study of electron spin relaxation at 4.2 K of free radicals in a single crystal of 4-methyl-2,6-ditertiarybutylphenol (MDBP) under the resonant condition that the electron Larmor frequency and the 4-methyl tunnelling frequency are equal. We compare the results to a theory which assumes a single tunnelling frequency throughout the sample for 4-methyl groups in molecules neighbouring free radicals. The reader is referred to Clough and Hobson (1974) for a general discussion of the quantum mechanical tunnelling of the 4-methyl group in MDBP. At these temperatures motion of the tertiarybutyl groups can be ignored.

A very low concentration of unpaired electron spins can be produced by γ -irradiation of MDBP which removes the phenol hydrogen atom to leave phenoxy radicals. Nuclear magnetic resonance (NMR) experiments indicate that the tunnelling frequency of methyl groups on undamaged molecules is about 9.4 GHz (Clough and Hobson 1974), although there is a distribution about this value (Clough and Hobson 1974, Nugent 1977). These results are confirmed by neutron scattering experiments (Clough and Heidemann 1977). At a magnetic field of about 0.34 T, the electron Larmor frequency is coincident with the tunnelling frequency and the coupling between the electron and methyl group thermal

† Present address: Department of Physics, Bryn Mawr College, Bryn Mawr, Pennsylvania, 19010, USA.

reservoirs has a profound effect on the electron spin relaxation. These effects were first observed by Clough and Hill (1975) (henceforth referred to as CH) and it is this paper which generated the interest leading to the present in depth study.

In the following section, we briefly discuss the general properties of electron spin relaxation in MDBP based on the model of CH. This leads to a set of coupled relaxation equations for the electron (on the damaged molecule) and its nearby methyl groups (on undamaged molecules). The magnetic coupling between the electron and the methyl groups is via the intermolecular dipole–dipole interaction between the electron and the three protons. This has been discussed thoroughly by Beckmann (1977) (henceforth referred to as BE) and we review this paper in § 2.2. We can neglect the 4-methyl group on the damaged molecule since the tunnelling resonance here occurs at the much lower frequency of 4.1 GHz (Clough and Hobson 1974). One of the results of the present study, however, is that there may be other interactions beside the dipole–dipole interaction discussed above involved in the electron spin relaxation process. In § 3, the experimental procedure and results are given and in § 4 we discuss the theoretical predictions for the relaxation process. First we outline a simple phenomenological model which does not quantitatively explain the experimental results but does give some physical insight into what is being done in a more detailed calculation. This more detailed calculation involves solving the coupled equations introduced in § 2. The predictions of these calculations are then compared with the experimental results in § 5 and a brief summary is given in § 6.

2. Review of previous work in MDBP

2.1. The CH relaxation model

At the resonant field, saturating the electron spin resonance (ESR) signal has the effect of transferring energy to the nearby methyl groups. This is because transitions become allowed in which an electron spin flips relative to an external magnetic field and a neighbouring methyl group simultaneously converts between the A and E nuclear spin symmetry species. With a sufficiently strong saturating field, the electron reservoir remains at infinite temperature during the saturation and this has the effect of heating the methyl groups in the vicinity of each electron. After the saturation, the electron temperature tends towards that of the lattice but must cool the methyl groups in the process. The methyl groups are not coupled to each other so a temperature will be associated with each group in equation (1). A discussion in thermodynamic terms is very convenient and is equivalent to a discussion of populations of the two methyl-group tunnelling states (i.e. of the proton spin symmetry species A and E) and the two electron m_s states. The effect of the electron–methyl-group coupling is striking as first observed by CH. The intrinsic or non-resonant electron relaxation rate R_s is $\gtrsim 1 \text{ s}^{-1}$ (CH) whereas, as indicated in § 3, the resonant rate of recovery from saturation is highly non-exponential varying from about 10^{-1} s^{-1} immediately after the saturation to about 10^{-3} s^{-1} at very long times. An important aspect of the relaxation process, verified dramatically by CH, is the fact that *the methyl groups are not coupled to the lattice* at 4 K, thus they can only relax via the electron. The electron, methyl-group and lattice reservoirs and the relevant couplings between them are indicated schematically in figure 1.

A single electron–methyl-group pair tends towards a common temperature independent of the lattice while conserving the total energy of the pair (equations (10) in CH). Since

the concentration of damaged molecules is very low, one assumes a model consisting of a single electron in a sea of methyl groups and the total coupling between the electron and its neighbouring methyl groups is obtained by summing over the methyl groups. Finally, one introduces the coupling between the electron and the lattice via the relaxation rate R_s discussed previously. With this model, CH arrived, in a straightforward

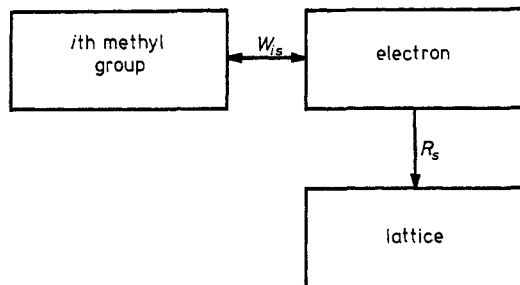


Figure 1. Schematic representation of the methyl-group, electron and lattice reservoirs. The couplings W_{is} and R_s are discussed in the text. The methyl groups do not interact with the lattice at 4 K.

manner, at the following coupled equations describing the recovery of the electron and methyl group reservoirs following a saturation pulse.

$$\begin{aligned} \frac{d}{dt}\beta_s &= -R_s\beta_s - \sum_i W_{is}(\beta_s - \beta_i) \\ \frac{d}{dt}\beta_i &= -W_{is}(\beta_i - \beta_s) \end{aligned} \quad (1)$$

Here, β_s and β_i refer to the departure from the equilibrium or lattice value of the inverse temperatures of the electron and the i th methyl group. The transition probability W_{is} depends on the distance of methyl group i from the electron and is discussed in the following section. The couplings W_{is} and R_s are indicated in figure 1.

2.2. The electron–methyl-group interaction

W_{is} is the transition probability per unit time for a change of methyl group tunnelling state ($A \leftrightarrow E$) accompanied by the simultaneous flip of an electron spin ($\Delta m_s = \pm 1$). The interaction responsible for the coupling is the intermolecular dipole–dipole interaction between the electron and the three protons in a methyl group. A detailed discussion and calculation of W_{is} which assumes a point dipole–dipole interaction between an electron and a methyl group proton can be found in BE (equations (31) and (32)). There are four angles that enter the problem; two specifying the orientation of the electron–methyl-group vector and two specifying the orientation of the magnetic field. The crystal and molecular structure of MDBP is well known (Maze and Rerat 1964, Maze-Baudet 1973). The crystal structure is orthorhombic with four molecules per unit cell; thus in a reference frame centred on the unpaired electron spin, there are only four sets of field angles but many sets of angles specifying the methyl groups. The electron, which is treated as a point dipole, is placed at the centre of charge of the damaged molecule (Nugent 1977). If a powder average is performed the relatively complicated expression

for W_{is} referenced above reduces to the fairly simple expression (BE, equation (37)) given by

$$W_{is} = \frac{5}{2} \gamma_e^2 \gamma_n^2 \hbar^2 \Delta^2 r_{is}^{-8} g(v_s - v_i) \quad (2)$$

where γ_e and γ_n are the gyromagnetic ratios of an electron and a proton, Δ is the distance from the centre of the triangle of protons in the methyl group to each proton and r_{is} is the distance from the electron to the methyl group. The assumption of the powder average is discussed further in §4. The smallest value of r_{is} (i.e. $i = 1$) is 5.19 Å and for comparison, $\Delta = 1.02$ Å.

A physical picture of the origin of the factor $(\Delta)^2 r_{is}^{-8}$ can be found in §3 of BE. The r_{is}^{-8} dependence of W_{is} is of central importance in the ESR relaxation process.

A more precise form of the distribution function $g(v)$ in equation (2) is $g(v_s - v_{t,i} - \Delta m_I v_n)$ where v_s , v_n and $v_{t,i}$ are the electron Larmor frequency, the proton Larmor frequency and the tunnelling frequency of the i th methyl group. As discussed in BE, $g(v)$ is, in general, a complicated convolution of the electron, nuclear and tunnelling frequency distributions. It is precisely the convolution that satisfies the resonant criterion $v_s - v_{t,i} - \Delta m_I v_n = 0$. In interpreting ESR experiments, the terms in v_n may be neglected since $v_n \ll v_s, v_{t,i}$. (This approximation is not valid in the interpretation of NMR experiments.) Also, since we are dealing with a single tunnelling frequency, $v_{t,i}$ is independent of i which labels the methyl groups. Under these circumstances, $g(v)$ becomes the ESR lineshape taken to be Gaussian and given by (33) in BE. If the crystal and molecular structure is known, which is the case for MDBP, and the electron is treated as a point dipole, numerical values of W_{is} can be computed *with no adjustable parameters*.

3. The relaxation experiments

The experiments were performed on a single crystal of MDBP at 4.2 K using an ESR cylindrical cavity. With suitable modifications, a Decca X-Band Spectrometer could be cavity locked at a series of frequencies between 8.9 and 9.7 GHz. The modulation intensity was set such that the structure associated with the normal seven line spectrum (Clough and Poldy 1969) was just integrated out although there was no further modulation broadening. The resulting ESR line is very well represented by a Gaussian of halfwidth 45.4 MHz. The derivative of the absorption was monitored in the normal way and the magnetic field was adjusted to coincide with one of the dispersion peaks. The experimental results were independent of which peak was used.

Each experiment was performed only after the methyl group reservoir was in thermodynamic equilibrium with the lattice. This took several thousand seconds after cool down or after each experiment. Different klystrons were used for the saturation pulse and for monitoring the recovery; their frequency being set the same by monitoring and eliminating their beat frequency. In order to achieve reliable results the level of the monitoring klystron was decreased until no saturation was observed over a period of about 10^3 s. It is here where the experiments differ from conventional ESR in that one is dealing with relaxation times of up to 10^3 s. The signal had to be monitored at extremely low levels of RF power resulting in relatively poor signal to noise.

As an aside, it should be noted that the experiment is somewhat different from that of CH since CH allowed partial saturation due to the observing microwave power to improve signal to noise. Thus, CH measured the recovery to a steady state, but not

thermal equilibrium value. As a result, the relaxation times CH report are much shorter than those reported here.

In the present experiment, the ESR signal is saturated (starting from thermal equilibrium at 4.2 K) with the high power klystron for a period of $t_a = 5, 50$ or 200 s. After the saturation is turned off, the recovery is monitored until the equilibrium signal has been well established. The total time for such a recovery depends on ν_s and t_a and was between 1000 and 4000 s. The time scale after the saturation is labelled by t_b (i.e. $t_b = 0$ at the end of the saturation pulse). Seventy-eight experiments of this form were performed in the range $8.97 < \nu_s < 9.63$ GHz. An example of such an experiment is shown in figure 2 and

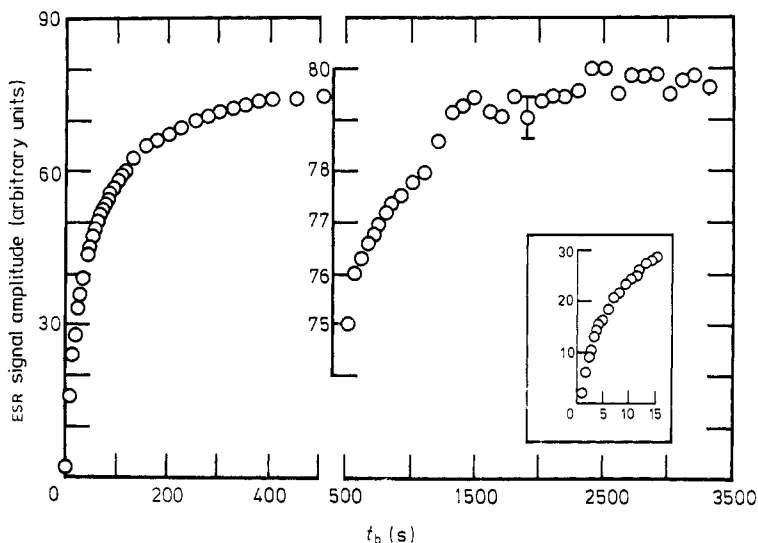


Figure 2. The recovery of the ESR signal following a $t_a = 200$ s saturation pulse at an ESR frequency of $\nu_s = 9.49$ GHz. At $t_b = 500$ s, the t_b scale is reduced by a factor of 4 and the signal scale is expanded by a factor of 10: 80 units being common to both scales. The inset shows the evolution during the first 15 seconds on a t_b scale expanded by a factor of 10.

the highly non-exponential nature of the relaxation is best seen by plotting the departure from equilibrium (which can be called β_s) on a semi-log plot which is done in figure 3. Exponential relaxation would manifest itself by a straight line on such a plot. In figure 2, the data points for $t_b < 100$ s (only a few of which are shown) are single measurements from the chart recorder whereas the data points in the regions $100 < t_b < 200$ s, $200 < t_b < 400$ s, $400 < t_b < 900$ s and $900 < t_b < 3300$ s are 15, 25, 50 and 100 s averages respectively. The error flag shows one standard deviation for the $t_b > 900$ s data points. All 78 measurements were analysed in a similar fashion. In figure 3 where the *departure* from the equilibrium ESR signal is plotted, the error flags include the sum of three uncertainties: the uncertainty discussed above, the statistical uncertainty associated with the ESR signal amplitude at time t_b (not shown in figure 2) and an error introduced by long-term DC drifts in the apparatus. The latter uncertainty, which is not negligible, was estimated by performing experiments under the same conditions for many hours.

In order to compare the solutions of the coupled relaxations equations (1) with the experimental results it is convenient to define a time dependent electron spin relaxation

rate $R_1(t_b)$ through the relation

$$\frac{d}{dt}\beta_s(t_b) = -R_1(t_b)\beta_s(t_b). \quad (3)$$

The parameter $R_1(t_b)$ is obtained in a straightforward manner from the slopes of tangents to the relaxation curves like that of figure 3. In general, R_1 will depend on the ESR frequency ν_s , the saturation time t_a , and the time t_b after the end of the saturation. The times

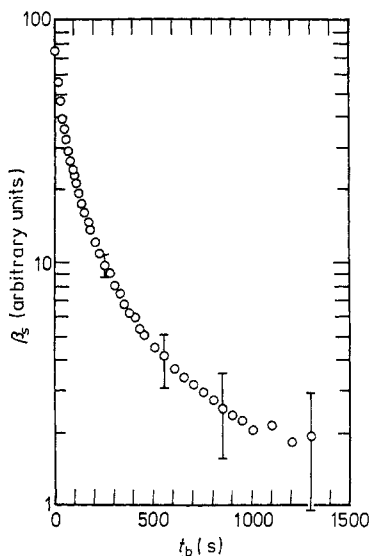


Figure 3. The departure from equilibrium of the ESR signal shown in figure 2. Exponential relaxation would be characterised by a straight line on this plot.

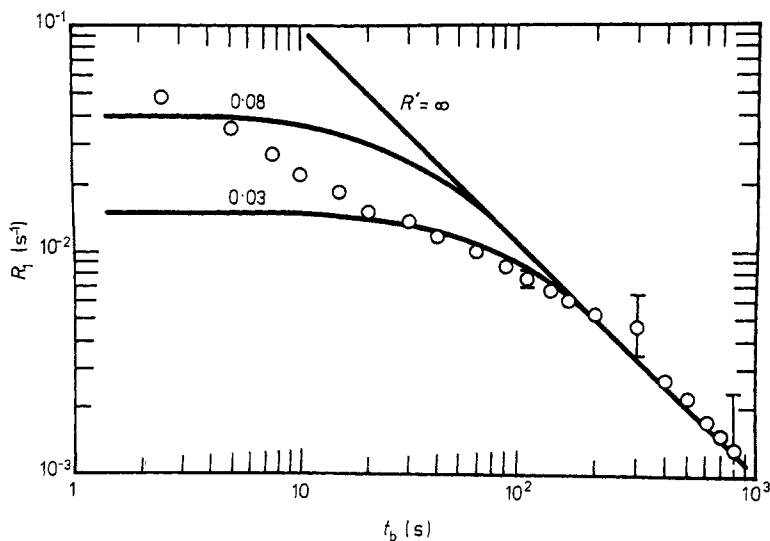


Figure 4. The electron relaxation rate R_1 versus t_b . The open circles are the experimental values for $\nu_s = 9.63$ GHz and $t_a = 200$ s. Exponential relaxation would be characterised by a horizontal line on this plot. The full curves are given by equation (5) in the text for the values of R' as shown.

t_a were chosen to be 2.5, 10, 32, 100, 250 and 400 s. Representative measurements of $R_1(\nu_s, t_a, t_b)$ are shown in figures 4 and 5 as a function of t_b for various values of ν_s and t_a as indicated. The full curves in these figures will be discussed later. Note that exponential relaxation would be characterised by horizontal lines in these figures. Thus, the observed electron spin relaxation is highly non-exponential.

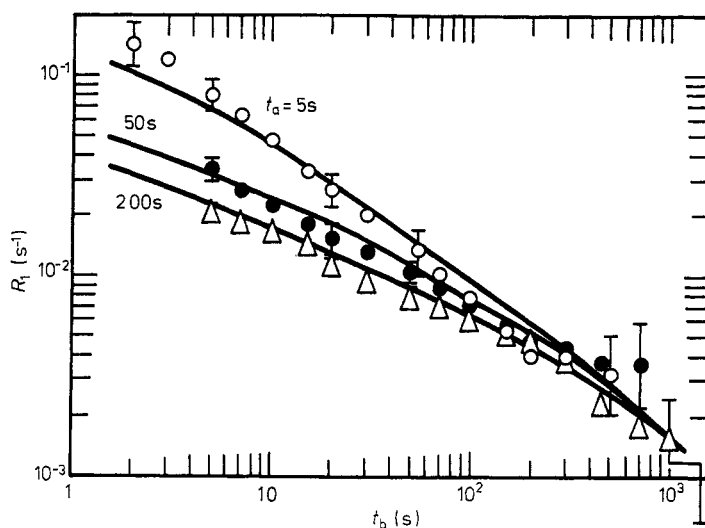


Figure 5. The electron relaxation rate R_1 versus t_b for $\nu_s = 9.33$ GHz and saturation times t_a as shown. The open circles, full circles and open triangles are the experimental values and the full curves are the theoretical predictions as discussed in §4 of the text.

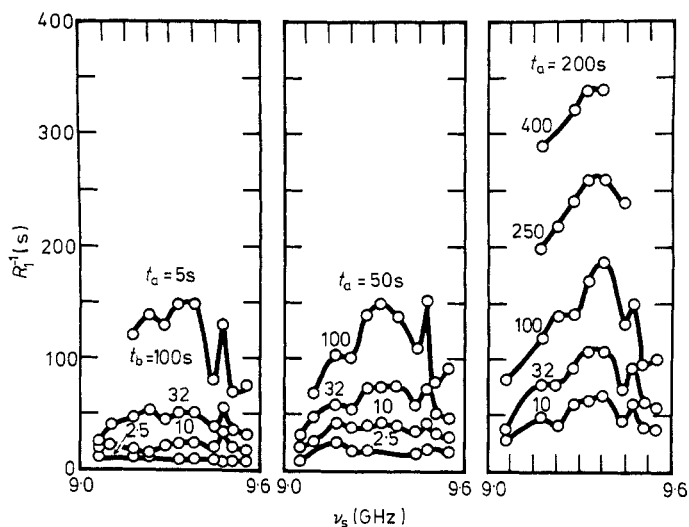


Figure 6. The experimental values of the electron relaxation time R_1^{-1} as a function of ESR frequency ν_s for fixed values of t_a and t_b . The three groups of data correspond to the three values of t_a as indicated and the different sets within each group correspond to different values of t_b as indicated. The full curves are visual aids only and have no theoretical basis. The top set in the middle group is shown in greater detail in figure 7.

All the experiments are summarised in figure 6 where each plot corresponds to R_1^{-1} versus ν_s for fixed t_a and t_b . The peak at the resonance condition $\nu_s = \nu_l = 9.4$ GHz is plainly seen. The full curves in figure 6 are for visual aid only and have no theoretical basis. Since the uncertainties in R_1 are appreciable in some cases these full curves must be treated with caution. One example of the 13 sets of data points in figure 6 is shown in figure 7. Note that R_1 is plotted in figure 7 whereas R_1^{-1} is plotted in figure 6. The uncertainties in $R_1(\nu_s, t_a, t_b)$ are of different origin for short and long values of t_b . For small t_b , where β_s decreases rapidly and R_1^{-1} is small, the error flags are dominated by short-term random noise. For large values of t_b , where β_s decreases slowly and R_1^{-1} is large, the signal can be averaged as discussed previously, and the error flags are dominated by the

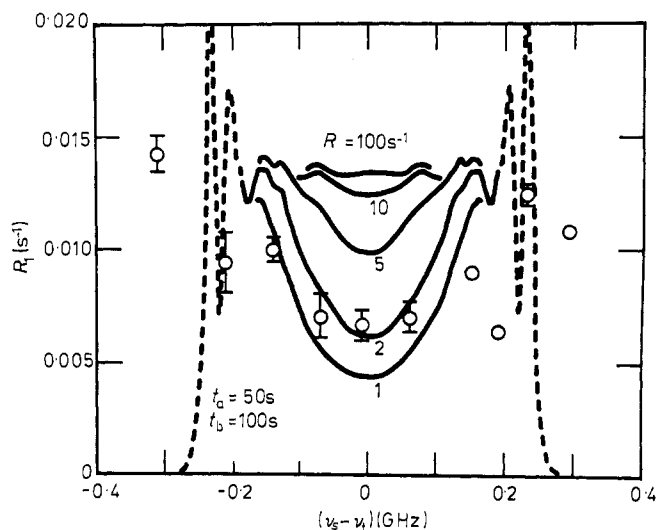


Figure 7. The electron relaxation rate R_1 versus $\nu_s - \nu_l$ for $t_a = 50$ s and $t_b = 100$ s. The uncertainties in the experimental values (open circles) are indicated where they are larger than the size of the open circles. The theoretical predictions, discussed in §4 of the text, are indicated by full and broken curves for different values of R_s as shown. Where only one line is shown, plots for all values of R_s coalesce to the same line. The theoretical predictions for fixed R_s are obtained as a function of $|\nu_s - \nu_l|$ with no adjustable parameters. Superimposing the experimental and theoretical values fixes $\nu_l = 9.34$ GHz in this case. The dashed portions indicate that β_s has decreased to less than 1% of its initial value and would thus be unobservable.

uncertainty in the infinity or equilibrium signal. This uncertainty is ultimately connected with the long-term instabilities of the apparatus. For small t_a values, in which case the relaxation is fast, it was not possible to determine R_1 for large values of t_b . For large t_a values, in which case the relaxation is slow, a longer measuring time constant was used which did not permit a determination of R_1 at small values of t_b . Between two and four experiments were performed for each ν_s, t_a and the spread in values of R_1 was consistent with the estimates of the uncertainties.

4. Theoretical predictions

Within the framework of a single tunnelling frequency model, the coupled equations (1)

can be solved for β_s or, via equation (3), for R_1 . First, however, we outline a very simple model which gives some insight into the origin of the non-exponential relaxation.

4.1. Simple phenomenological model

The non-exponential relaxation comes about because there are many relaxation rates in the relaxation process; namely R_s and all the W_{is} . Because the W_{is} are proportional to r_{is}^{-8} , these individual relaxation rates span a very large range. In general, the observed R_1 will be a suitably weighted sum over R_s and the W_{is} and $\beta_s(t_b)$ may be written

$$\beta_s(t_b) = \int_0^\infty f(R) e^{-Rt_b} dR. \quad (4)$$

Equation (4) is phenomenological and $f(R)$ is a normalised distribution of relaxation rates. Perhaps the simplest choice for $f(R)$ is $f(R) = \text{constant}$ for $R \leq R'$ and $f(R) = 0$ for $R > R'$. An upper limit R' to the allowed values of R is certainly reasonable although the step function approximation is very crude. It is easily shown that in this case

$$R_1(t_b) = \frac{1}{t_b} - \frac{R' e^{-R't_b}}{1 - e^{-R't_b}} \quad (5)$$

which is plotted in figure 4 for three values of R' . At long times the first term in equation (5) dominates whereas in the limit $t_b \rightarrow 0$, $R_1 \rightarrow \frac{1}{2}R'$. It is perhaps not surprising that at long times this crude model agrees with the experimental results very well since any realistic model for $f(R)$ must tend to zero for large R and one will always obtain a t_b^{-1} dependence. It is interesting that at long times R_1 equals t_b^{-1} , i.e. the constant of proportionality is unity. (See also the experimental results in figures 4 and 5.) At shorter t_b values, the solutions to equation (4) are sensitive to the form of $f(R)$ and the crude approximation leading to equation (5) gives poor agreement with experiment as shown in figure 4.

Although the predictions at long t_b tend to confirm the multirelaxation rate model, it is not possible to incorporate the dependence of v_s, v_t, t_a and the molecular and crystal parameters of MDBP into such a simple model. To do this, we must solve the coupled relaxation equations (1) using numerical techniques.

4.2. Detailed numerical solutions

The parameters required to solve the coupled equations (1) are; the transition probabilities W_{is} , the initial conditions and R_s . The transition probabilities W_{is} can be calculated on a computer for each methyl group i . A detailed study of the solutions to equations (1) with and without the powder average was performed and the result is that the sets of solutions agreed to better than 2% under all conditions of interest. That the angles specifying the electron-methyl-group vector do not play a significant role is not surprising as discussed in BE but that the field angles do not play a significant role is perhaps somewhat surprising. This was checked experimentally by changing the orientation of the crystal with respect to the applied magnetic field. The single crystal, then, behaves as if it were a powder because of the large number of methyl groups involved. Within the framework of a single tunnelling frequency model the W_{is} in equation (2) can be calculated with no adjustable parameters as a function of $|v_s - v_t|$ since $g(v)$ in equation (2) is just the Gaussian ESR lineshape given by equation (33) in BE.

The initial conditions for $\beta_s(t_b)$ and $\beta_i(t_b)$ in the coupled equations (1) are given by

$$\begin{aligned}\beta_s(0) &= -\beta'_i \\ \beta_i(0) &= -\beta'_i[1 - \exp(-t_a W_{is})]\end{aligned}\quad (6)$$

where β'_i is the inverse lattice temperature and β_s and β_i are the departures from β'_i of β'_s and β'_i the inverse temperatures of the electron and the i th methyl group. The only assumption is that $\beta'_s = 0$ during the saturation; i.e. the electron relaxation is negligible. From the known W_{is} , the initial conditions are easily determined with no adjustable parameters. Examples of such a computation are shown in figure 8. This indicates the radius

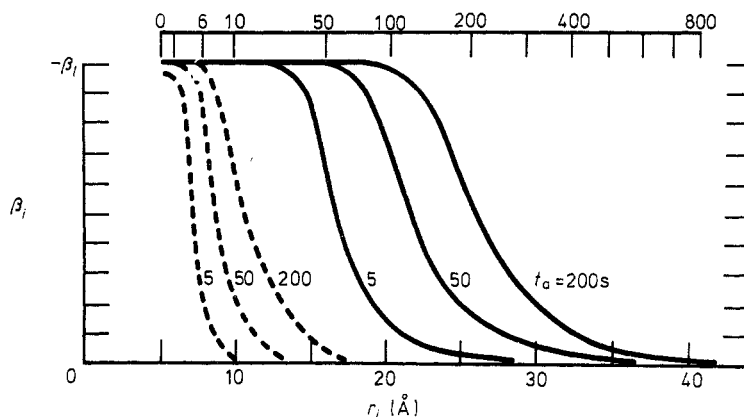


Figure 8. The initial conditions $\beta_i(0)$ given by equation (6) in the text. The methyl groups are ordered with respect to distance and the plots correspond to $|v_s - v_t| = 0$ (full curves) and 0.2 GHz (broken curves) and to different values of t_a as indicated. The distance r_i is measured from the centre of charge of the damaged molecule which contains the unpaired electron spin. The number of methyl groups as a function of distance is obtained from the top and bottom axes.

of the hot 'bubble' surrounding each free radical following the saturation. The case for $t_a = 200$ s and $|v_s - v_t| = 0$ corresponds to the situation where the most methyl groups are influenced by the saturation (i.e. $t_a = 200$ s was the longest saturation employed in the experiment).

The coupled equations (1) can be solved, (subject to the initial conditions) for β_s (and the β_i) or, via equation (3), for R_1 by diagonalising the appropriate $(n + 1) \times (n + 1)$ matrix for the electron and n methyl groups. The number of methyl groups employed in the calculation was 878 which includes all the groups within a distance of 42 Å of the electron. In practice, a much smaller matrix was diagonalised by squashing the distant groups into shells. This was done by ordering the W_{is} ($i = 1$ to 878) in decreasing order and setting all the W_{is} in a certain range W to $W + \delta W$ to the same value. The details of the procedure are complicated and great care was taken to ensure the final solutions were insensitive to the approximations employed. Because of the r_{is}^{-8} dependence of W_{is} , it is surprising that so many methyl groups had to be included in the calculations. Reducing the number to 338 (all those within 30 Å) led to significantly different values of R_1 at long t_b values.

The parameter R_s is the only adjustable parameter and it is known to be ≥ 1 s⁻¹. We found that values of R_s between 1 and 3 s⁻¹ fit the experimental data quite well in

the region $|v_s - v_t| < 0.15$ GHz, this frequency being more than 3 times 45 MHz, the halfwidth of the ESR line.

The results, then, of the numerical calculations are the theoretical predictions of $R_1(|v_s - v_t|, t_a, t_b)$. An example of R_1 versus t_b for $v_s - v_t = 0$ for various values of t_a is given in figure 5. Note that R_1 approaches t_b^{-1} independent of t_a in agreement with the simple theory presented in §4.1. In principle, at least, the distribution function $f(R)$ could be determined but this could only be done numerically and would be of little value. Examples of R_1 versus $|v_s - v_t|$ for fixed t_a and t_b are shown in figure 7.

5. Comparison between theory and experiment

In the range $v_s \sim v_t$, the experimental results and the theoretical predictions agree very well, the non-exponential shape of the saturation recovery being in accord with calculation. Since the theoretical values are functions of $|v_s - v_t|$, superimposing theoretical plots on the experimental results specifies v_t which, in the case of figure 5, is $v_t = 9.33$ GHz since the theoretical plot corresponds to $|v_t - v_s| = 0$ and the experimental values to $v_s = 9.33$ GHz. This value of v_t is very close to the value of the centre of the tunnelling frequency distribution as measured by NMR techniques (Clough and Hobson 1974). If the intrinsic or non-resonant electron relaxation rate R_s is treated as a parameter for one of the three plots in figure 5 (i.e. one value of t_a) then the predicted values of R_1 for the other two are obtained with no adjustable parameters. The agreement is therefore very satisfactory since it indicates that not only is the non-exponential recovery shape explained by the theory but also the dependence of that shape on the saturation time. We note that there is considerable curvature in the experimental and theoretical log-log plots in figure 5 which means we are not in the long t_b limit where $R_1 = t_b^{-1}$ until the very largest t_b values shown. The value of R_s used in the theoretical plots in figure 5 was 2 s^{-1} . The experimental results between 9.2 and 9.4 GHz could all be fitted successfully on an individual basis but not all together for the same values of v_t and R_s . The ranges were $9.2 < v_t < 9.5$ GHz and $1 < R_s < 3 \text{ s}^{-1}$. Since we know there is a distribution in the tunnelling frequency distribution and since R_s may possibly be frequency dependent, the failure to find a unique fit for all the experiments $9.2 < v_s < 9.4$ GHz is not surprising. The main conclusion here is that the shape of the relaxation curve (i.e., R_1 versus t_b) and the dependence on t_a is adequately explained by the theoretical predictions in the range $|v_s - v_t| < 0.15$ GHz.

The major role played by the factor $|v_s - v_t|$ is the number of groups with which the electron effectively communicates within the time scale set by t_a and t_b . This can be seen in figure 8 where, for example, about 10 groups are affected by a $t_a = 200$ s saturation pulse for $|v_s - v_t| = 200$ MHz but many hundreds are affected for $|v_s - v_t| = 0$. Thus the further one goes from the central tunnelling frequency, the more sensitive the experiments are to the distribution of tunnelling frequencies. As can be seen in figure 7, the agreement between theory and experiment in the region $|v_s - v_t| > 0.15$ GHz is generally poor. This corresponds to ESR frequencies greater than about 9.5 GHz and less than about 9.2 GHz since v_t is assigned the value 9.34 GHz in these plots. The combination of the general agreement between theory and experiment for $|v_s - v_t| < 0.15$ GHz and the poor agreement for $|v_s - v_t| > 0.15$ GHz indicates that the general relaxation model is correct but that a more realistic model of the tunnelling frequency is required.

When the resonance condition is not met the relaxation of the electron is expected to be almost independent of the methyl groups. The saturated ESR signal should therefore

recover in the order of five seconds to 99% of the equilibrium value and the rate of recovery at later times would hardly be measurable. For this reason the calculated values of R_1 for large values of $|\nu_s - \nu_l|$ are shown by broken lines in figure 7 since they would be inaccessible to measurement. In practice the recovery remains relatively slow even when $|\nu_s - \nu_l|$ is of the order of 0.4 GHz. This is clearly seen in figure 6. Obviously this can be accounted for by supposing that there exists a distribution of tunnelling frequencies so that the resonance condition is satisfied at all frequencies ν_s for at least some methyl groups. The saturation recovery is then slowed in proportion to the number of resonant groups.

The NMR measurements also indicate a distribution of tunnelling frequencies which is well described by a Gaussian function with a full width at half maximum of 0.4 GHz. The peaks observable in figure 6 are quite consistent with this result. It seems likely that the distribution is broader for those methyl groups located close to free radicals since local strains due to radiation damage may affect the tunnelling frequency. This would explain why the peaks in figure 6 are better developed for the long values of t_b which reflect the tunnelling frequency distribution relatively far from the free radicals. Though relaxation is closer on resonance than off, the difference is less than anticipated from the NMR measurements. It may be that phonon assisted energy transfer occurring off resonance is responsible for this broadening.

The evidence strongly points to a distribution of tunnelling frequencies over a range of the order 0.4 GHz. This has the important consequence of reducing the number of methyl groups which are resonant when $\nu_s = 9.4$ GHz by a factor of about six. Then, the agreement between the theoretical and experimental saturation recovery curves requires $R_s^{-1} = \frac{1}{3}$ rather than 2. This is not in good agreement with the measured value of R_s^{-1} at 7 GHz.

This suggests that if the value $R_s^{-1} \sim 2$ is correct at 9.4 GHz then each electron interacts with more methyl groups than can be accounted for by the magnetic dipole-dipole interaction. The only candidate for a relatively long-range interaction would seem to be a virtual phonon interaction. The Larmor precession of the electron is accompanied by lattice motion which modulates the magnetic dipole-dipole interaction of a neighbouring methyl group leading to an interaction of electrons and methyl groups because both are coupled to the phonons. Such interactions are certainly small, but the present method of measurement, involving as it does times of the order 10^3 – 10^4 s, is capable of detecting extremely small interactions. This interesting possibility is the subject of current experiments.

6. Concluding remarks

We have measured the electron spin relaxation in MDBP at eleven frequencies between about 9.0 and 9.6 GHz for various saturation times. An important improvement (aside from measuring at more than one frequency) over the preliminary experiments of CH is that we have measured the true relaxation curves; i.e. the recovery to the equilibrium signal rather than to a non-equilibrium, steady-state signal (due to partial saturation by the monitoring process). This results in highly non-exponential relaxation characterised by time constants of a few seconds at short times after the saturation to a thousand seconds, in some cases, at very long times after the saturation.

Two important advances have been incorporated in this work. First, the probabilities associated with the intermolecular electron-methyl-group dipole-dipole interaction

have been calculated with no adjustable parameters. Secondly, the crystal and molecular structure of MDBP has been incorporated explicitly into the calculations.

In the region $\nu_s \sim \nu_t$, the evolution of the ESR signal amplitude following saturation and the dependence of this evolution on the time of the saturation is adequately explained by the theory which has one adjustable parameter for three sets of recovery curves corresponding to the different saturation times. We feel that this agreement firmly establishes the model whereby the electron is coupled to a sea of methyl groups.

There is marked disagreement between theory and experiment in the frequency dependence of the electron relaxation rate R_1 for $|\nu_s - \nu_t| \gg \bar{\nu}_s$ where $\bar{\nu}_s$ is the half width of the ESR signal. This disagreement is mainly resolved by introducing a distribution of tunnelling frequencies which has the effect of diminishing the difference between resonant and non-resonant experiments. The implication of this though is that the electron-methyl-group interaction is stronger and of longer range than is accounted for by a pure dipole-dipole interaction. Identification of other interaction mechanisms is an important problem for the future.

Acknowledgments

We sincerely thank Dr Jethro Hill for his help with the ESR equipment and Dr Stuart Nugent who patiently taught us how to use the molecular and crystal structure parameters of MDBP. This work was supported by the Science Research Council (UK) and the National Research Council of Canada.

References

- Beckmann P A 1977 *Molec. Phys.* **34** 665-80
- Clough S and Heidemann A 1977 *Proc. Int. Symp. on Neutron Inelastic Scattering, Vienna*
- Clough S and Hill J R 1975 *J. Phys. C: Solid St. Phys.* **8** 2274-82
- Clough S and Hobson T 1974 *J. Phys. C: Solid St. Phys.* **7** 3387-402
- Clough S and Poldy F 1969 *J. Chem. Phys.* **51** 2076-84
- Maze-Baudet 1973 *Acta Crystallogr. B* **29** 602-14
- Maze M and Rerat C 1964 *C.R. Acad. Sci., Paris* **259** 4612-5
- Nugent S M 1977 *J. Phys. C: Solid St. Phys.* **10** 781-9